Electronic Supplementary Information

Simultaneous Achievement of Defect Passivation and Carrier Transport Promotion by Emerald Salt for Methylammonium-Free Perovskite Solar Cells

*Zhenghui Fan,[a] Yuan Yin,[b] Bing Cai, *[a] Qingshan Ma,[a] Qianlong Liu,[a] Xinhang Liu,[a] Yinhua Lv,*[a] and Wen-Hua Zhang,*[acd]*

[a] Institute of Chemical Materials, China Academy of Engineering Physics, 596 Yinhe Road, Chengdu 610200, China

[b] College of Physics and Optoelectronic Technology, Baoji University of Arts and Sciences, Baoji 721016, P.R. China

[c] Yunnan Key Laboratory of Carbon Neutrality and Green Low-carbon Technologies, School of Materials and Energy, Yunnan University, Kunming 650500, China

[d] Jiangsu Collaborative Innovation Center for Photovoltaic Science and Engineering, Changzhou University, Changzhou 213164, P. R. China.

* Corresponding Author

E-mail: bingcai@caep.cn (B. Cai), qiehahah@163.com (Y. Lv), whzhang@caep.cn and wenhuazhang@ynu.edu.cn (W. -H. Zhang)

1.Experiment

1.1 Materials. All the solvents and reagents were used as received without further purification. Emeraldine salt (ES) and cesiumiodide (≥99.9%) were purchased from Sigma-Aldrich. Lead iodide, Lead Chlorine, $HC(NH_2)_2I$(FAI), $HC(NH_2)_2Br$ (FABr), and 2,2',7,7'-Tetrakis [N, N-di(4-methoxyphenyl) amino]-9,9'-spirobifluorene (Spiro-OMeTAD) were purchased from Xi'an Polymer Light Technology Corp. All the solvents were purchased from Aladdin. ITO glass substrates were purchased from SuZhouShangYang Solar Technology Co., Ltd.

1.2 Device fabrication. ITO glasses were cleaned in sequence with water, ethanol, acetone, and 2-propanol in an ultrasonic bath. The 13 mg/mL of SnO_2 nanocrystalline in ethanol solution was spin-coated on ITO substrate at 2000 rpm for 30s, the annealed at 150 °C for 30 min.[1] The precursor solution was prepared by mixing 53 mg of CsI, 186 mg of FAI, 591 mg of PbI_2, 19 mg of $PbCl_2$, 8 mg of FABr in 1 mL of DMF and DMSO solution (4:1, v/v). For ES-modified perovskite, the prepared ES solution (dissolved in the mixture solution of DMF and DMSO (4:1, v/v) over 24h with a concentration of 0.3 mg/mL) was blended with the perovskite precursor solution to obtain precursor solutions with different ES concentrations. The perovskite solution was spin-coated onto the compact SnO_2 films at 1000 and 4000 rpm for 10 and 30 s, respectively, in a nitrogen filled glovebox. After 110 μL of anisole was dropped onto the substrate in the 30th s, the substrate was annealed at 110 °C for 15 min. After cooling down to room temperature, hole transport material (HTM) solution was spin coated onto perovskite films at 5000 rpm for 30 s, where the solution was prepared by dissolving 72.3 mg of Spiro-OMeTAD, 28.8 μL of 4-tert-butylpyridine and 17.5 μL of Li-TFSI/acetonitrile (520 mg/mL) into 1 mL of chlorobenzene. Finally, 80 nm of gold electrodes were deposited by thermal evaporation.

For the large-area structured PSCs, the modules were fabricated in the configuration of FTO/compact TiO_2 (c-TiO_2)/mesoporous TiO_2 (mp-TiO_2) /Perovskite /Spiro-OMeTAD/ Au. Clean FTO glasses (5×5 cm^2, patterned by laser P_1 with a power of 16 W) were treated with UV-O_3 for 20 min prior to use. The c-TiO_2 layer was deposited by spray pyrolysis using a titanium diisopropoxide bis(acetylacetonate) solution at 450 °C. Both mp-TiO_2 and perovskite layers were

fabricated via a blade-coating method. For the mp-TiO_2 layer, 50 μL of TiO_2 paste (Dyesol 30NRD, diluted in ethanol) was bladed linearly at a speed of 4 mm/s, and annealed at 500 ℃ for 1 h. Before transferring into a N_2-filled glovebox, the substrates were treated with UV-O_3 for 20 min. 50 μL of 1.35 M perovskite solution ($Cs_{0.15}FA_{0.85}PbI_{2.85}Br_{0.05}Cl_{0.1}$ in DMF:NMP, 95:5, v:v) was bladed linearly at a speed of 4 mm/s. The wet films were blow-dried immediately by a compressed N_2 flow and then annealed at 110 ℃ for 15 min. The spiro-OMeTAD layer was spin-coated at 4000 rpm for 40 s. The mp-TiO_2, perovskite, and spiro-OMeTAD layers were scribed with laser P_2 (2.4 W). Then, an 80-nm-thick Au counter electrode was deposited by thermal evaporation. Finally, the as-prepared devices were scribed with laser P_3 (3.6 W) to complete the series connection. The width of the dead area (P1 to P3) and a single sub-cell are 0.9 and 5.4 mm, respectively. Thus, the geometrical FF (GFF) can be calculated as 83.1%.

1.3 Characterizations. The UV-vis spectra were measured using an Evolution™ 201 spectrophotometer (Thermo fisher scientific Corporation). The top-view SEM images were obtained by using a Zissis field-emission scanning electron microscope. The XRD was measured on Maxima 7000 diffractometer (Shimadzu, Japan) with a Cu *Ka* radiation (40 kV, 100 mA). The atomic force microscope (E-Sweep/Nano Navi; Yamato Scientific) were used to study the morphology and conductivity. The steady PL spectra and time-resolved PL decay measurements were performed using a HORIBA Delta Flex system (HORIBA) with an excitation wavelength at 510nm.The current-voltage characteristics were measured by Keithley 2400 source and the solar simulator with standard AM 1.5G (100mW·cm^{-2}, SS-F5-3A: Enlitech) under ambient conditions. The active area of the solar cells was confirmed by using a metal aperture of 0.09 cm^2 to avoid light scattering through the sides. The *J-V* curves were measured by forward (-0.1 to 1.2 V) or reverse (1.2 to -0.1 V) scans with a delay time of 10 ms for each point. Monochromatic external quantum efficiency (EQE) spectra were recorded as functions of wavelength with a monochromatic incident light of 1 ×10^{16} photons cm^{-2} in alternating current mode with a bias voltage of 0 V (QE-R3011). The light intensity of the solar simulator was calibrated by a standard silicon solar cell provided by PV Measurements. The electrochemical impedance Spectroscopy (EIS) and Mott-Schottky (M-S) analysis were conducted by using a multi-channel

potentiometer (VMP3, Biologic). EIS data were recorded in the frequency range from 1 MHz to 50 mHz with an AC amplitude of 50 mV. A contact angle measuring instrument (Shanghai Zhongchen Digtal Techology Apparatus Co. Ltd.) was used to measure the water contact angles. FTIR spectra were measured with an attenuated total refraction (ATR) spectrometer (thermo fisher scientific) from 4,000 to 400 cm^{-1} with are solution of 2 cm^{-1}. The energy band structure of samples was evaluated by ultraviolet photoemission spectroscopy (UPS) (Thermo Scientific, Escalab 250Xi). The assessments of the moisture and thermal stability of the solar cells (without encapsulation) were carried out by repeating the *J–V* characterizations at various times. For the moisture stability test, the devices were stored in an air-glovebox with controlled humidity. For the thermal stability test, the devices were stored in a N_2-glovebox, and heated with a hotplate. Series resistance (*R*s) was roughly evaluated by calculating the slope of the tangent line for *J-V* curves (reverse scan) at the open circuit voltage, according to the equation ($Rs=-\Delta V_{OC}/\Delta J_{OC}$).

1.4 DFT calculations. All the calculations were executed based on density functional theory method (DFT)[2], as implemented in the Vienna ab-initio simulation package (VASP). To simulate the interaction between the cores and valence electrons of all atoms in these systems, the projector augmented wave (PAW) pseudopotential was adopted[3]. We employed the generalized gradient approximation (GGA) of Perdew-Burker-Ernzerhof (PBE)[4] as electronic exchange-correlation functional. The kinetic energy cutoff of the plane-wave basis was set to 300 eV and the k-point meshes with grid spacing of 1 × 1 × 1 has been adopted. All the structures were fully relaxed until the total energy and force per atom were less than 10^{-4} eV and -0.01 eV/Å, respectively.

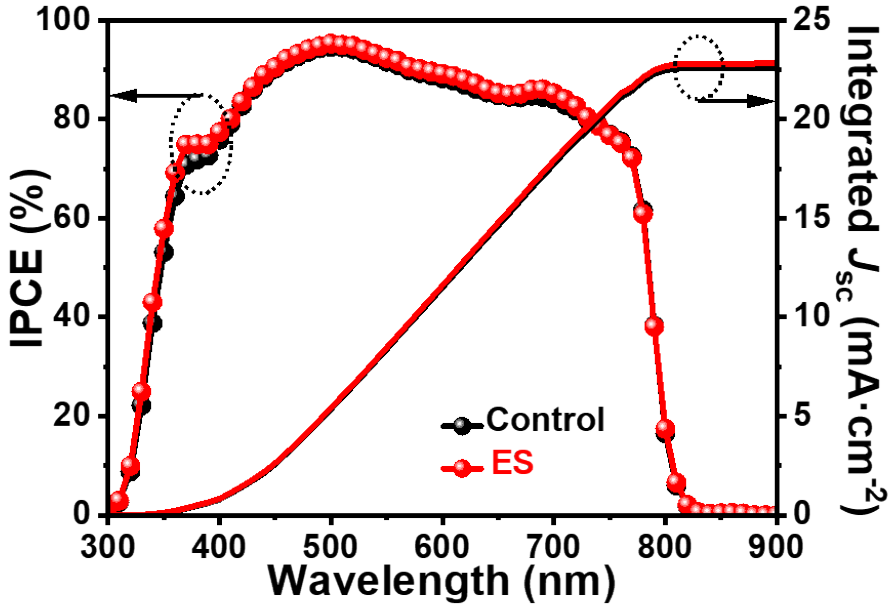

Fig. S1. EQEs and the integrated current density of the control and ES modified PSCs.

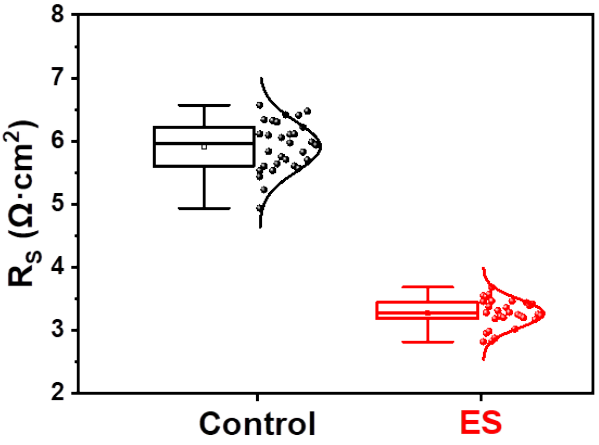

Fig. S2 Series resistance (R_s) of control and ES-based PSCs obtained from the *J-V* tests in **Fig. 1b**.

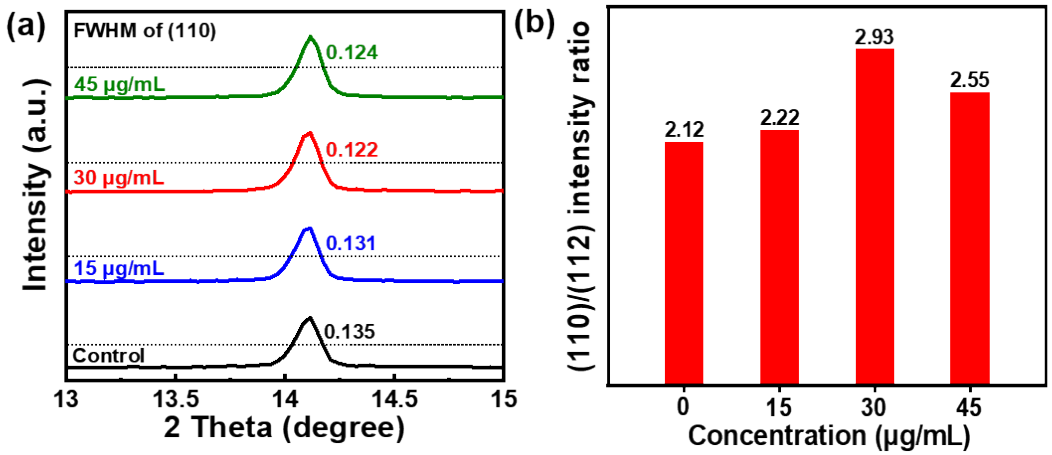

Fig. S3. (a) The full width at half maximum (FWHM) of (110) diffraction peak. (b) Diffraction peaks intensity ratios of the (110)/(112) planes derived from Fig. 2a.

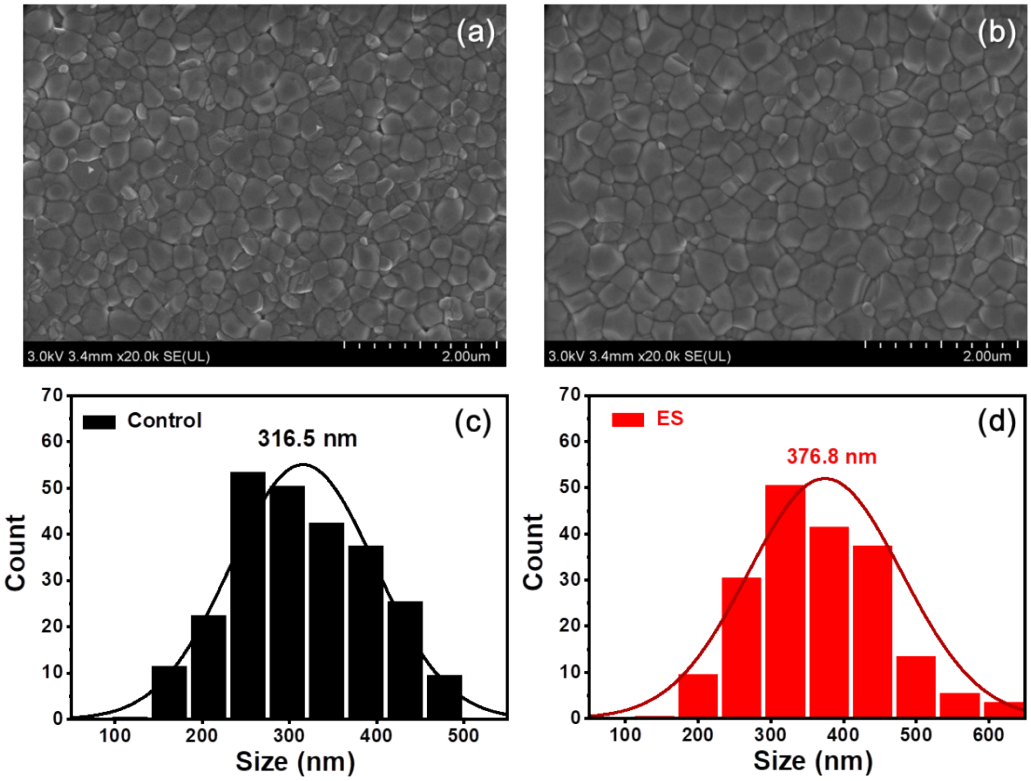

Fig. S4 SEM images and grain size distribution of perovskite films (a, c) without and (b, d) with ES.

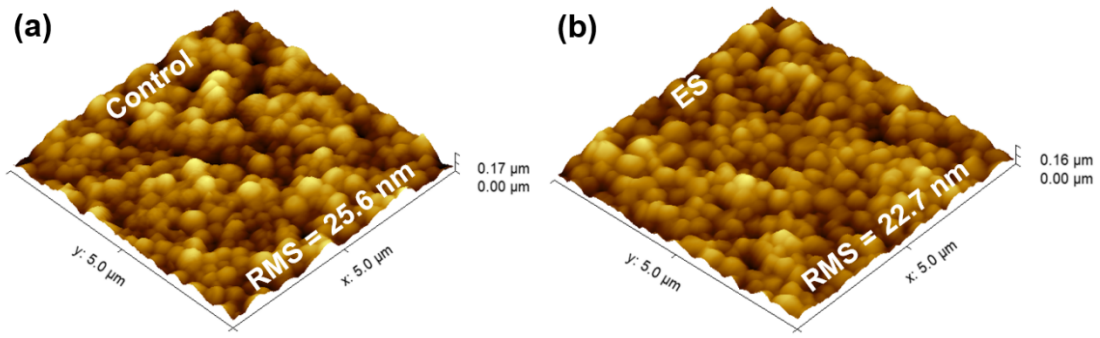

Fig. S5. The root-mean-square (RMS) roughness of perovskite films (a) without and (b) with ES.

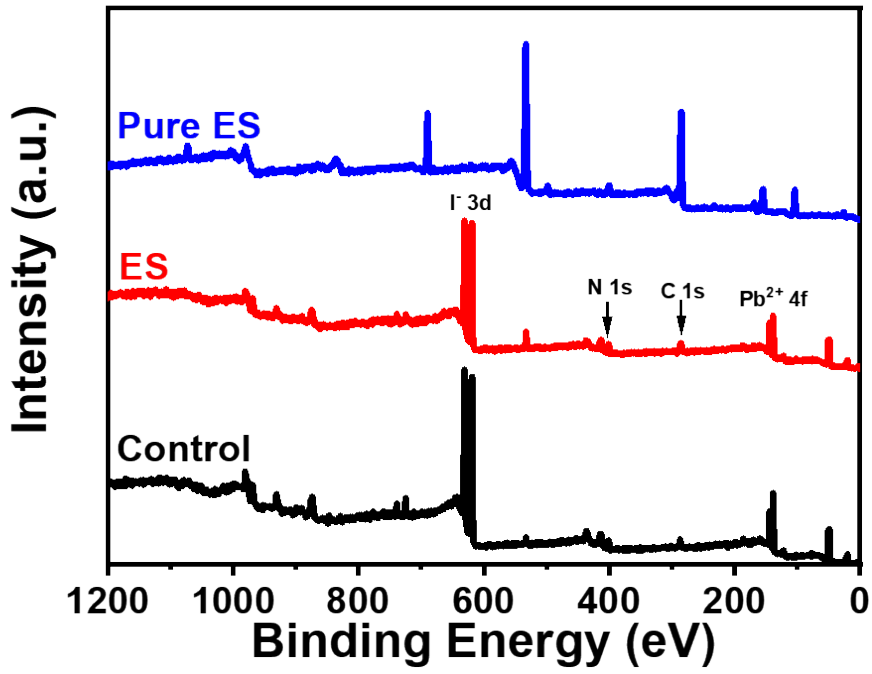

Fig. S6. Survey XPS spectra of ES, the ES-based, and the control perovskite films.

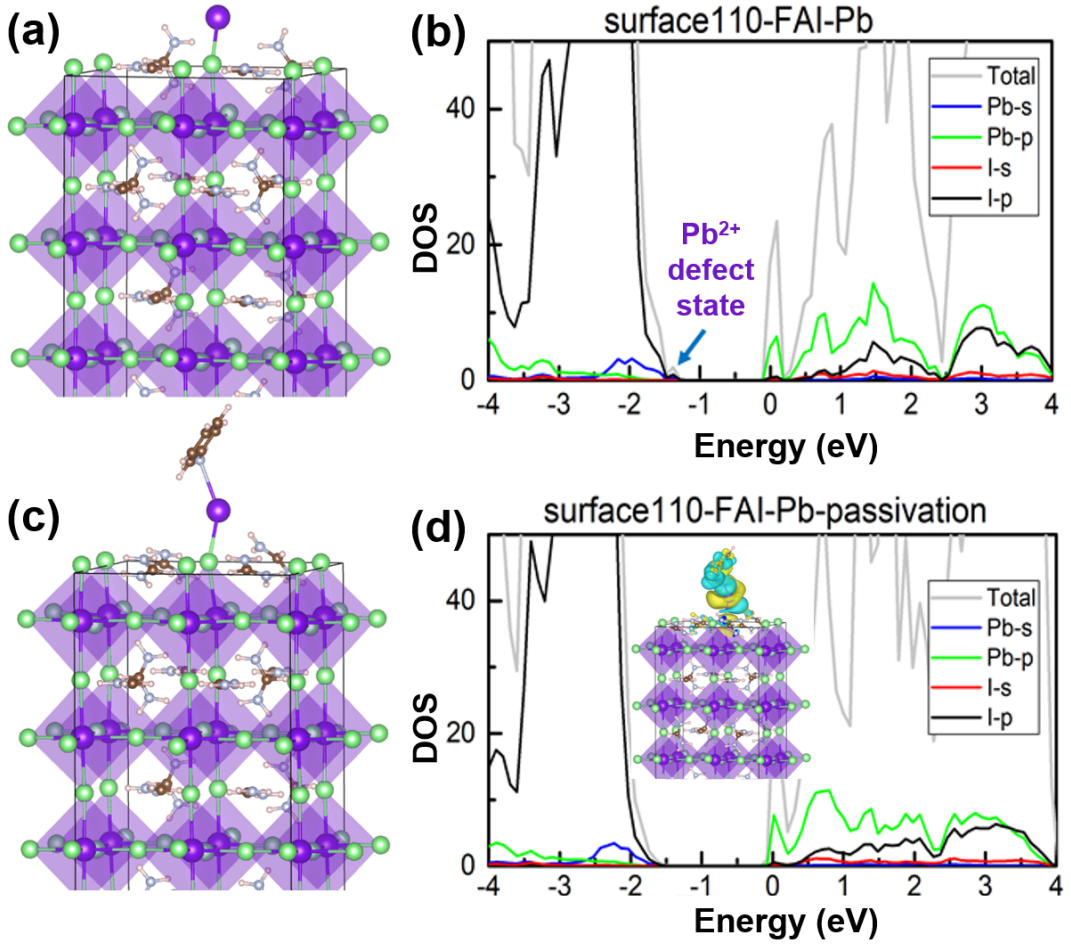

Fig. S7. DFT calculation results: (a) Optimized crystal structure and (b) density of states (DOS) of defect Pb^{2+} on surface (110) of FAI-termination. Corresponding passivation results are shown in (c) and (d), respectively.

First-principle calculations were employed to explore the passivation mechanism of ES on the perovskite surface. Defects Pb^{2+} and I^- were all taken into consideration, and no defect state was produced on surface (110) of both FAI-termination and PbI_2-termination of defect I^-. It can be found that defect state was created beyond the valence band maximum (VBM) as shown in **Fig S6**b. And this defect level disappeared after ES incorporation (**Fig S6**d), demonstrating the effective passivation of defects by ES.

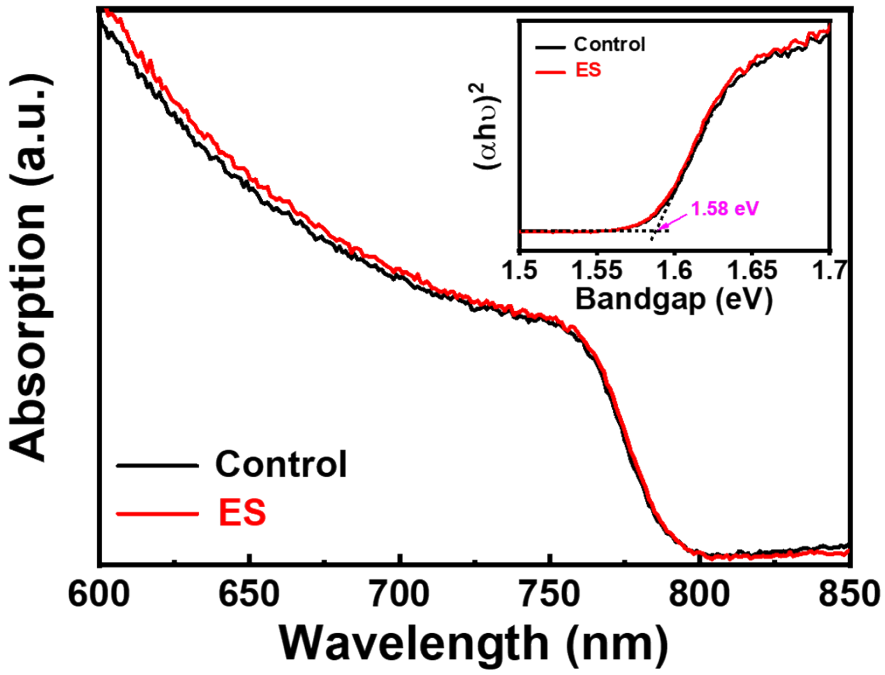

Fig. S8. The UV-vis absorption spectra of control and ES perovskite films (inset: the corresponding bandgaps of 1.58 eV).

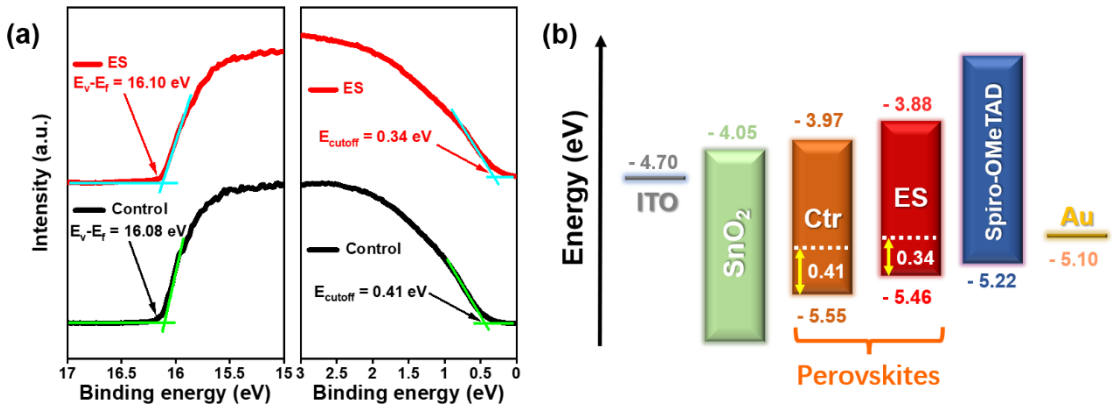

Fig. S9. (a) The UPS spectra. (b) The corresponding energy levels.

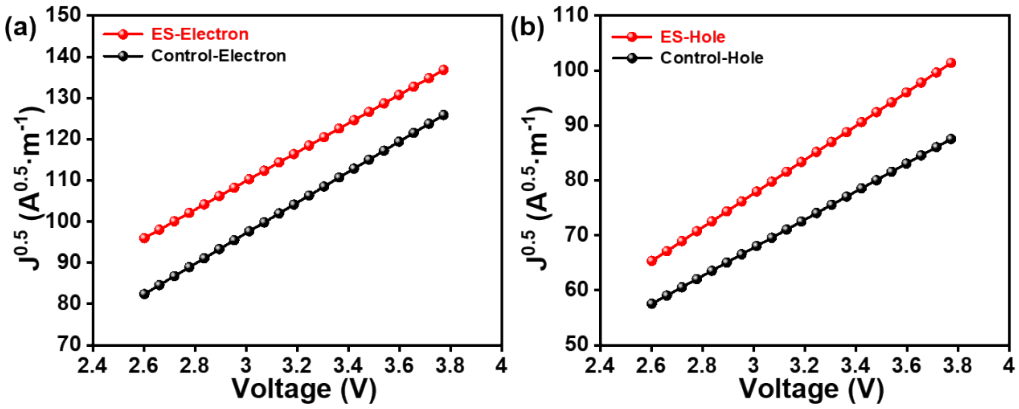

Fig. S10. $J^{0.5}$-V plots for the (a) electron-only and (b) hole-only devices based on control and ES perovskites.

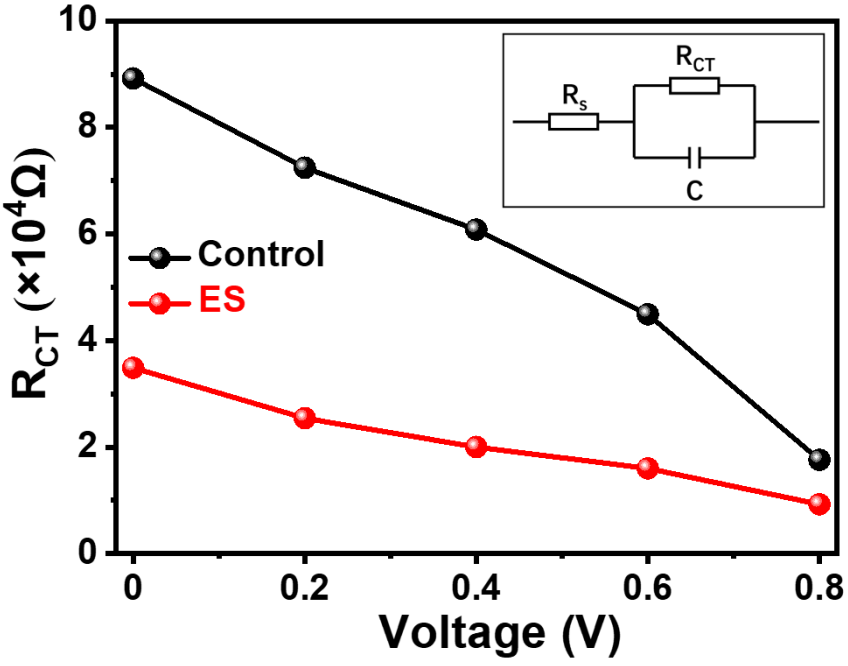

Fig. S11. The dependence of R_{CT} on applied bias voltage according to the EIS plots in Fig. 6c, d. The inset is the equivalent circuit model.

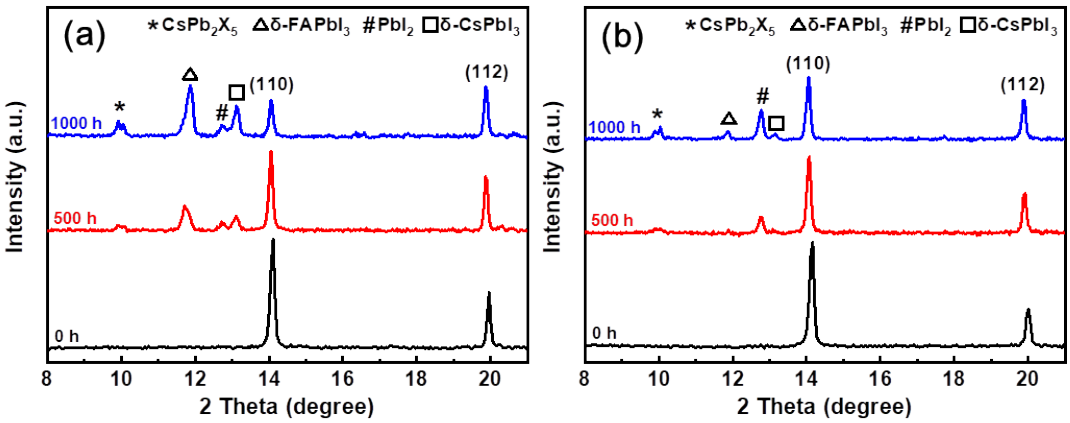

Fig. S12 XRD patterns change over time for perovskite films (a) without and (b) with ES additive stored in moist air with RH 35±5%

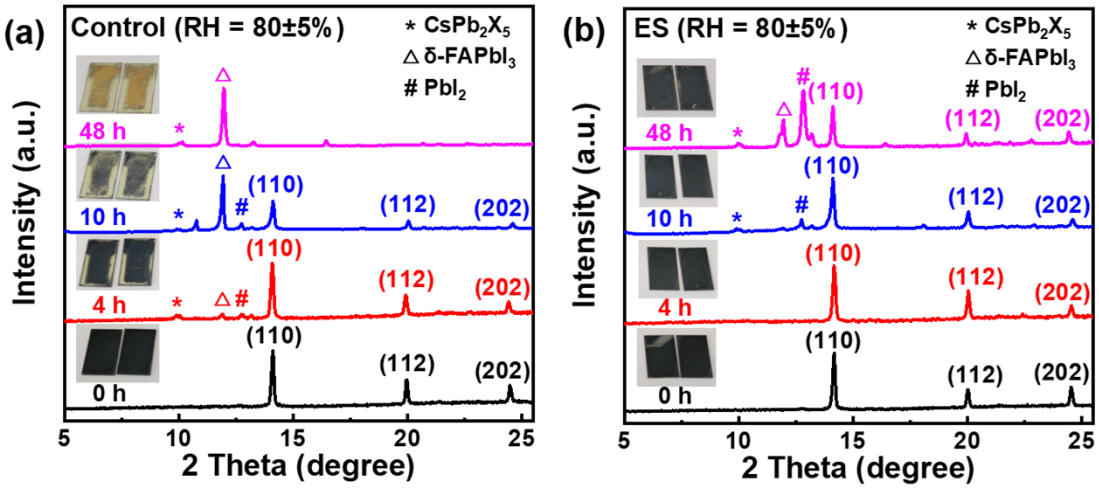

Fig. S13 Photographs of morphological changes over time of the perovskite films when subject to a RH condition of 80±5% and their corresponding XRD patterns change over time.

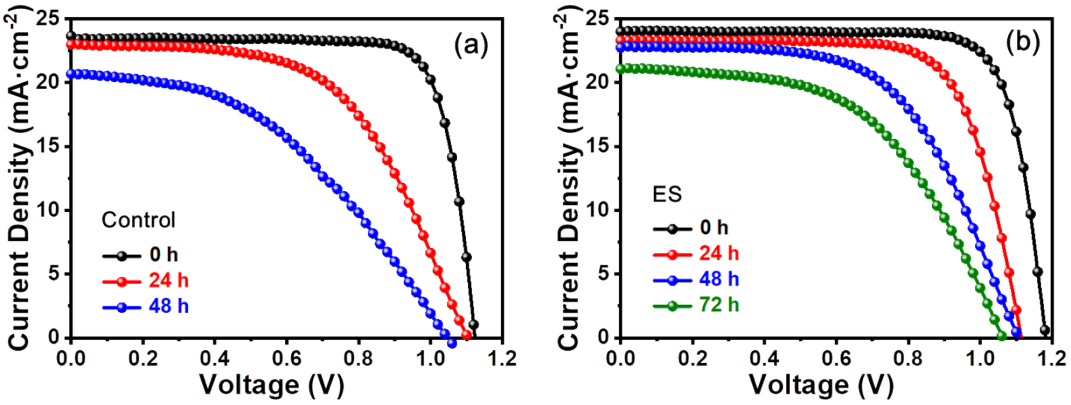

Fig. S14 *J-V* curves for (a) control and (b) ES-based PSCs stored in humidity air with RH 80±5%

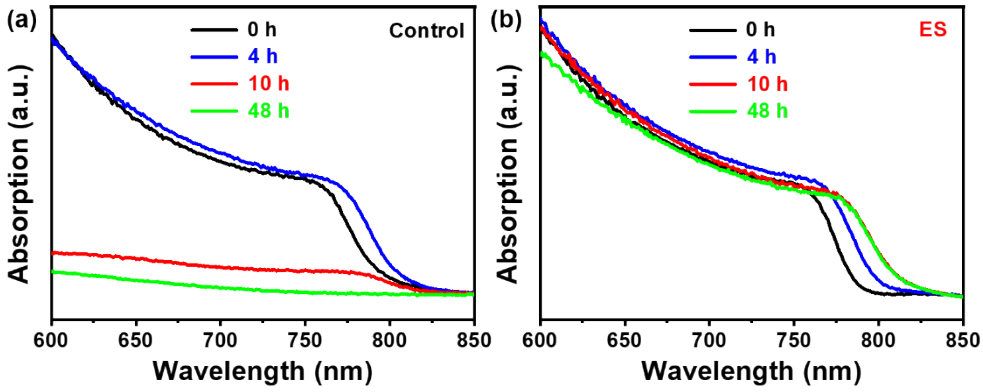

Fig. S15. The changes in UV-vis absorption spectra of (a) control and (b) ES-based perovskite films when subject to an RH condition of 80±5% for varied periods.

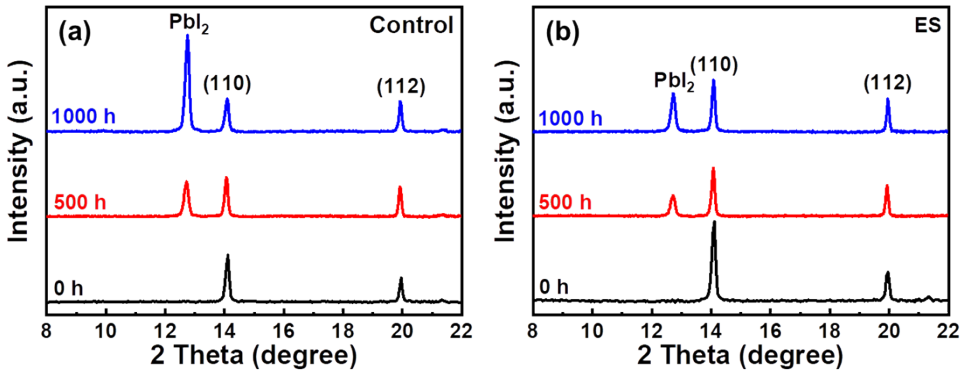

Fig. S16 XRD patterns change over time for perovskite films (a) without and (b) with ES additive under 85°C thermal stress.

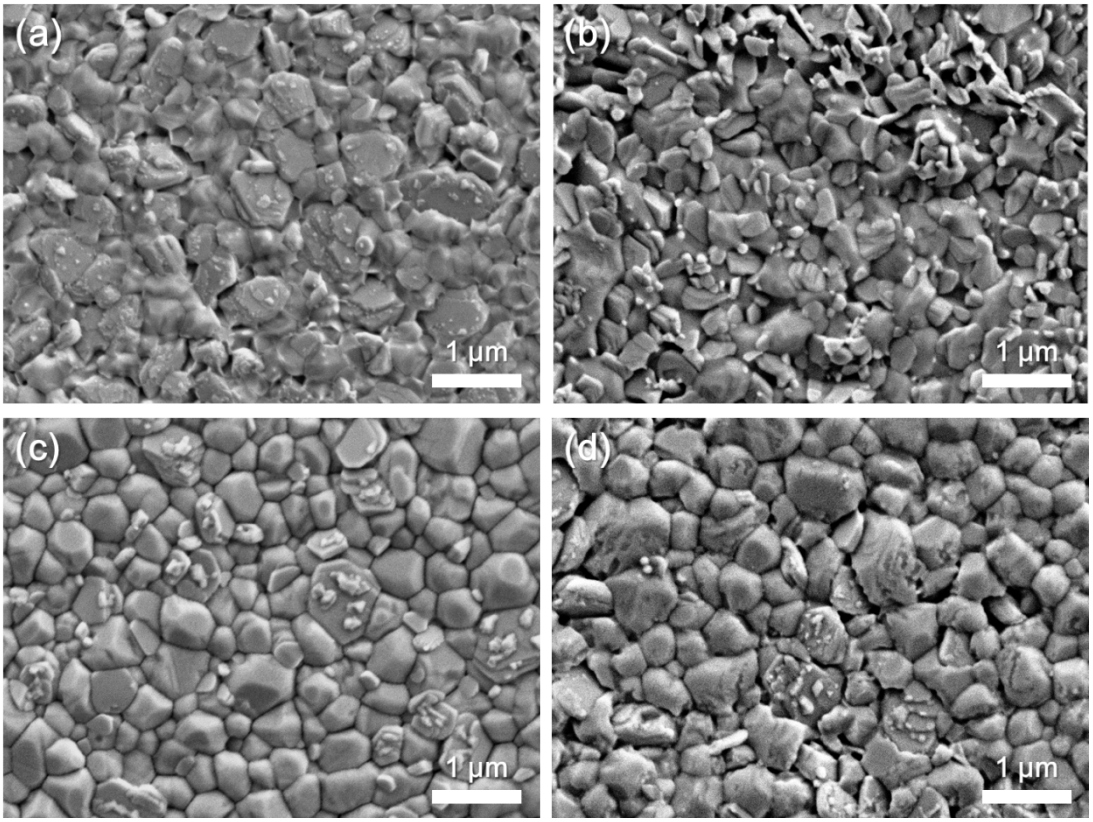

Fig. S17 Top view SEM images of perovskite films (with/without ES) heated at 85 °C for different times. (a) Control, 500 h. (b) Control, 1000 h. (c) ES, 500 h. (d) ES, 1000 h.

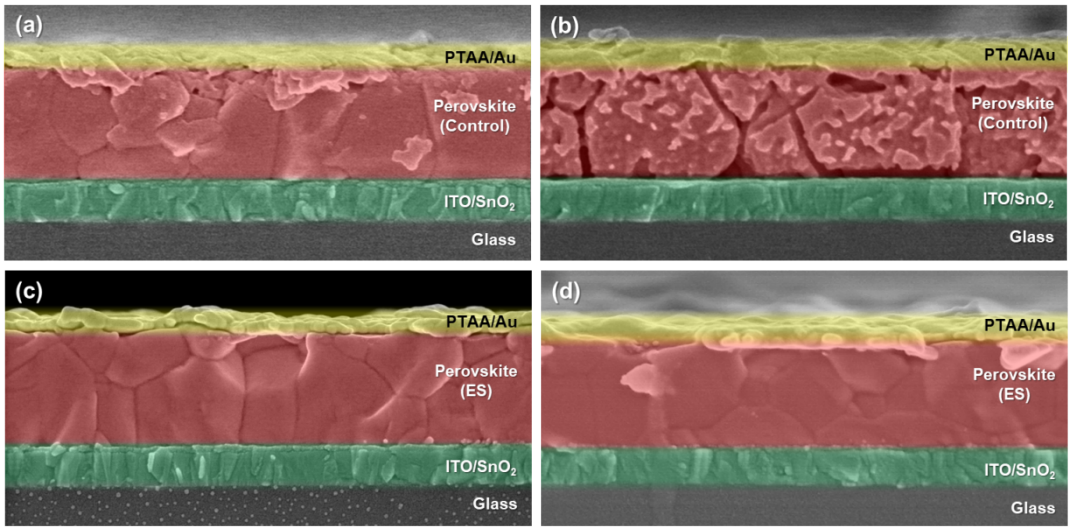

Fig. S18 Cross-sectional view SEM images of perovskite films (with/without ES) heated at 85 ºC for different times. (a) Control, 500 hours, (b) Control, 1000 hours, (c) ES, 500 hours, (d) ES, 1000 hours.

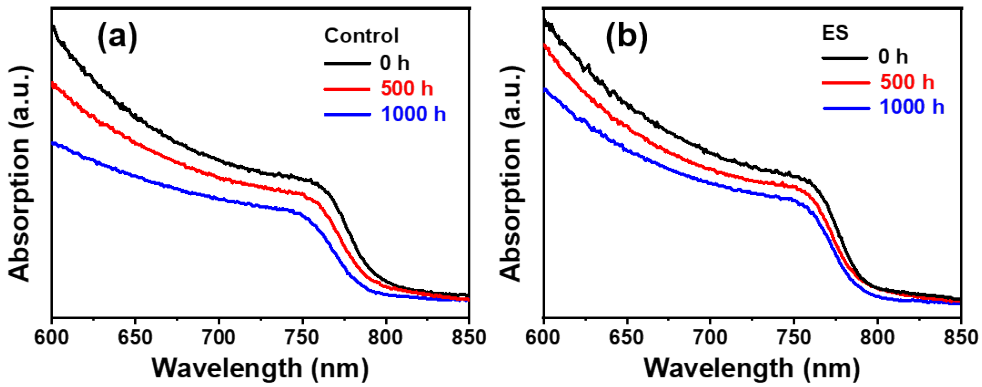

Fig. S19. The changes in UV-vis absorption spectra of (a) control and (b) ES-based perovskite films when subject to an condition of 85℃ for varied periods.

Table S1. Reported PSCs modified by polyaniline additives.

Year	Polyaniline	Device structure	PCE (Control)	PCE (Target)	Ref.
2018	C-PANI (conductive polyanilines, acidified by HBr/HI)	FTO/c-TiO_2/mp-TiO_2/$MAPbI_3$(with or without additive)/carbon	7.92%	9.40%	5
	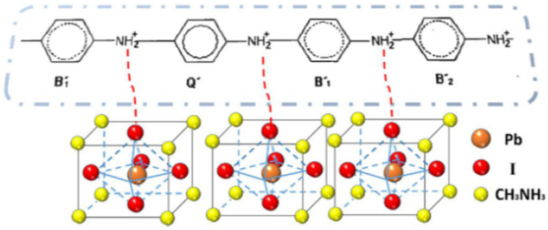				
2019	PANI (reduced state, emeraldine salt)	FTO/c-TiO_2/mp-TiO_2/ $(FAPbI_3)_{0.85}$ $(MAPbBr_3)_{0.15}$ (with or without additive)/spiro/Au	16.96%	19.09%	6
	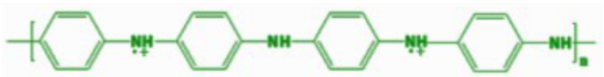				
2020	PANI (conductive state)	FTO/SnO_2/$CsPbI_2Br$ (with or without additive)/carbon	9.50%	13.52%	7
	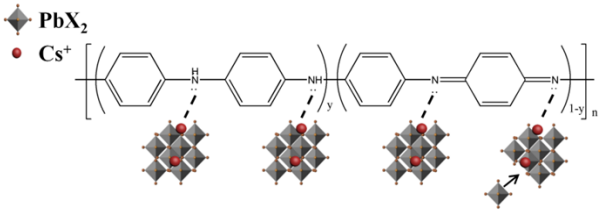				
2022	ES (emeraldine salt)	ITO/SnO_2/FACsPbIBr (with or without additive)/spiro/Au	21.5%	23.00%	This work
	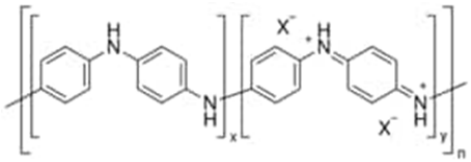				

Table S2. Summary of PV performance for n-i-p structured MA-free PSCs (including forward and backward scan).

Year	Device structures	V_{OC} (V)	J_{SC} (mA·cm^{-2})	FF (%)	PCE (%)	Ref.
2016	FTO/c-TiO_2/**$Cs_{0.15}FA_{0.85}PbI_3$**/Spiro/Ag	1.08	21.5	75	17.30	8
		-	-	-	-	
2016	FTO/c-TiO_2/mp-TiO_2/**$Cs_{0.2}FA_{0.8}PbI_{2.84}Br_{0.16}$**/Spiro/Au	1.07	21.9	74.2	17.35	9
		-	-	-	-	
2016	FTO/SnO_2/PCBM/**$Cs_{0.17}FA_{0.83}Pb(I_{0.6}Br_{0.4})_3$**/Spiro/Ag	1.2	19.4	75.1	17.10	10
		-	-	-	-	
2016	FTO/SnO_2/C_{60}-SAM/**$Cs_{0.2}FA_{0.8}PbI_3$**/Spiro/Au	1.09	22.25	80.85	19.57	11
		1.05	22.01	78.25	18.12	
2017	FTO/PCBCB/**$Cs_{0.17}FA_{0.83}Pb(I_{0.8}Br_{0.2})_3$**/Spiro/Au	1.07	22.1	80	18.80	12
		-	-	-	-	
2017	FTO/c-TiO_2/PCBM/**$Cs_{0.1}FA_{0.9}PbI_{2.865}Br_{0.135}$**/Spiro/Au	1.04	23	80.5	19.30	13
		1.01	23.2	73.5	17.20	
2017	FTO/c-TiO_2/**BA:$Cs_{0.15}FA_{0.85}Pb(I_{0.73}Br_{0.27})_3$**/Spiro/Au	1.24	19.83	73.7	18.13	14
		1.24	19.77	64.1	15.71	
2017	FTO/SnO_2/C_{60}-SAM/**$Cs_{0.2}FA_{0.8}Pb(I_{0.7}Br_{0.3})_3$**/Spiro/Au	1.25	18.53	78.95	18.27	15
		1.21	18.54	74.40	16.62	
2018	FTO/c-TiO_2/**$Cs_{0.2}FA_{0.8}Pb(I_{0.95}Br_{0.05})_3$**/Spiro/Au	1.12	22.82	78.82	20.05	16
		1.08	22.61	74.78	18.20	
2018	FTO/c-TiO_2/mp-TiO_2/**$(FAPbI_3)_{0.88}(CsPbBr_3)_{0.12}$**/**$(5\text{-}AVA)_2PbI_4$**/CuSCN/Au	1.07	21.93	72	16.75	17
		1.02	21.89	67	14.97	
2018	FTO/c-TiO_2/**$Cs_{0.17}FA_{0.83}Pb(I_{0.6}Br_{0.4})_3$**/Spiro/Au	1.23	18.34	79	17.80	18
		-	-	-	-	
2018	FTO/c-TiO_2/**Sb^{3+}:$Cs_{0.1}FA_{0.9}PbI_3$**/Spiro/Ag	1.10	22.85	84	21.04	19
		1.09	22.83	83	20.65	
2018	FTO/SnO_2/PCBM/PMMA/**$Cs_{0.1}Rb_{0.05}FA_{0.85}PbI_3$**/PMMA/Spiro/Au	1.08	25.06	75.5	20.44	20
		1.05	24.91	70.0	20.35	
2018	FTO/SnO_2/**$Cs_{0.17}FA_{0.83}PbI_{2.7}Br_{0.3}$**/Spiro/Au	1.14	23.2	80	21.10	21
		-	-	-	-	
2018	FTO/EDTA-SnO_2/**$Cs_{0.05}FA_{0.95}PbI_3$**/Spiro/Au	1.11	24.57	79.2	21.60	22
		1.11	24.55	78.3	21.34	
2018	FTO/TiO_2/**$FA_{0.9}Cs_{0.1}PbI_{2.9}B_{r0.1}$**/Spiro/Au	1.04	23.0	78.0	18.56	23
		1.03	22.6	76.30	17.75	
2019	FTO/TiO_2/C_{60}/**$FA_{0.9}Cs_{0.1}PbI_3$**/Spiro/Au	0.99	22.32	74.82	16.39	24
		0.98	22.24	70.54	15.50	
2019	FTO/c-TiO_2/mp-TiO_2/**$CEA_{0.05}(Cs_{0.1}FA_{0.9})_{0.95}Pb(I_{0.9}Br_{0.1})_3$**/Spiro/Au	1.10	22.77	79.91	20.08	25
		1.09	22.48	79.73	19.53	

2019	FTO/ZnO/$Cs_{0.17}FA_{0.83}Pb(I_{0.83}Br_{0.17})_3$/ Spiro/Ag	1.20 -	22.50 -	78.1 -	21.10 -	26
2019	FTO/c-TiO_2/mp-TiO_2/$(Cs_{0.05}FA_{0.95}PbI_3)_{0.94}(CsPbBr_3)_{0.06}$/ Spiro/Au	1.145 1.151	24.52 24.47	77.5 72.9	21.78 20.54	27
2019	FTO/c-TiO_2/mp-TiO_2/ $Cs_{0.2}FA_{0.8}PbI_{2.64}Br_{0.36}$/Carbon	1.08 1.05	20.1 20.1	66.4 58.5	14.50 12.3	28
2020	FTO/c-TiO_2/mp-TiO_2/ mp-ZrO_2/$Cs_{0.1}FA_{0.9}PbI_3$/Carbon	0.92 -	23.63 -	69 -	15.00 -	29
2020	FTO/c-TiO_2/mp-TiO_2/ **HMII-FAPbI$_3$**/Spiro/Au	1.07 -	24.85 -	78 -	20.60 -	30
2020	ITO/SnO_2/$(EDACl_2)_\omega(Cs_{0.15}FA_{0.85}PbI_3)$/ Spiro/Ag	1.15 1.15	24.11 23.50	71.05 72.60	19.68 19.57	31
2020	FTO/c-TiO_2/ $Cs_{0.15}FA_{0.85}Pb(I_{0.9}Br_{0.1})_3$-PbS/Spiro/Au	1.15 1.12	23.06 23.07	79.82 77.55	21.07 20.07	32
2020	FTO/SnO_2/**FAPbI$_3$:PbS**/Spiro/Au	1.11 -	21.5 -	75.7 -	18.00 -	33
2020	FTO/c-TiO_2/ $Cs_{0.15}FA_{0.85}Pb(I_{0.9}Br_{0.1})_3$(Cl)/Spiro/Au	1.18 1.14	22.57 22.74	80.09 77.47	21.30 20.11	34
2020	FTO/c-TiO_2/mp-TiO_2/SnO_2/ $Cs_{0.17}FA_{0.83}Pb(I_{0.82}Br_{15}Cl_{0.03})_3$/Spiro/Au	1.12 -	23.28 -	78.33 -	20.50 -	35
2020	FTO/SnO_2/ZnO/ ***β*-GUA-$Cs_{0.05}FA_{0.95}PbI_3$**/ Spiro/Au	1.14 -	24.41 -	79.60 -	22.20 -	36
2021	ITO/SnO_2/$Rb_{0.02}$ $(FA_{0.95}Cs_{0.05})_{0.98}PbI_{2.91}Br_{0.03}Cl_{0.06}$/MTDA A/Spiro/Au	1.16 1.15	22.97 22.98	82.2 80.1	21.92 21.29	37
2021	ITO/SnO_2/**FAPbI$_3$**/Spiro/Ag	1.08 -	24.38 -	75.1 -	19.71 -	38
2021	FTO/SnO_2/ $Cs_{0.16}FA_{0.84}Pb(I_{0.88}Br_{0.12})_3$/Spiro/Au	1.02 0.98	22.4 22.2	78.6 77.6	18.0 16.9	39
2021	ITO/ZnO/ $Cs_{0.15}FA_{0.85}Pb(I_{0.9}Br_{0.1})_3$/Spiro/Ag	1.16 1.12	22.88 21.79	79.65 75.44	21.15 18.41	40
2021	FTO/ c-TiO_2/mp-TiO_2/ $Cs_{0.1}FA_{0.9}PbI_3$/Spiro/Au	1.01 0.94	25.21 23.82	78.61 71.92	20.05 16.13	41
2021	ITO/SnO_2/ D-J (BDA) $FA_4Pb_5I_{16-x}Br_x$/Spiro/Au	1.11 0.95	19.69 18.98	76.8 65.0	16.75 13.78	42
2021	ITO/SnO_2/$Rb_{0.02}(FA_{0.95}Cs_{0.05})Pb$ $I_{2.91}Br_{0.03}Cl_{0.06}$/ MTDAA/Spiro/Au	1.16 1.13	22.97 22.22	82.2 81.0	21.92 20.26	43
2021	FTO/ c-TiO_2/ $Cs_{0.15}FA_{0.85}PbI_{2.85}Br_{0.05}Cl_{0.1}$/Spiro/Au	1.163 1.139	23.54 23.52	81.97 78.78	22.4 21.1	44
2021	FTO/SnO_2/ **3D-$FA_{0.83}Cs_{0.17}PbI_3$** /2D-PVSK/Spiro/Au	1.178 1.175	24.03 24.06	82.5 81.8	23.35 23.13	45

2022	FTO/c-TiO_2/PCBA:PS/ **$FA_{1-y}MA_yPbI_{1-x}Br_x$**/TPAI/Spiro/Au	1.144	25.61	80.9	23.7	46
		1.105	25.52	68.4	19.3	
2022	Glass/FTO/*c*-TiO_2/*mp*-TiO_2/**$K_{0.05}Rb_{0.05}Cs_{0.10}FA_{0.80}PbI_3$**/Spiro/Au	1.121	24.86	80.83	22.53	47
		1.116	24.71	78.84	21.74	
2022	Glass/FTO/SnO_2/HADI/ **$FA_{0.9}Cs_{0.1}PbI_3$**/Spiro /Au	1.20	24.85	83.11	24.79	48
		1.16	24.78	79.20	22.71	
2022	Glass/FTO/SnO_2/OP/**$(Rb_{0.02}(FA_{0.95}Cs_{0.05})_{0.98}PbI_{2.91}Br_{0.03}Cl_{0.06})$**/Spiro/Au	1.12	24.82	79.48	22.09	49
		1.12	24.85	78.23	21.77	
2022	Glass/ITO/SnO_2/**$FA_{0.9}Cs_{0.1}PbI_3$**/ Spiro /Au	1.172	24.57	80.76	23.25	50
		1.161	24.63	79.38	22.70	
2022	ITO/SnO_2/**$FA_{0.9}Cs_{0.1}PbI_3$**/ Spiro /Ag	1.072	25.2	78.9	21.3	51
		1.059	25.1	78.1	20.8	
2022	FTO/TiO_2/**$Cs_{0.15}FA_{0.85}Pb(I_{0.95}Br_{0.03}Cl_{0.02})_3$**/ $(TFPA)_2PbI_4$/Spiro /Ag	1.15	24.2	82.0	22.7	52
		1.13	23.8	80.3	21.7	
2022	glass/ITO/SnO_2/**$Cs_xFA_{1-x}PbX_3$**/ spiro/MoO_3/Ag	1.16	25.24	81.7	23.9	53
		1.15	25.17	81.5	23.6	
2022	ITO/SnO_2/**$Cs_{0.1}(GABA_{0.075}FA_{0.925})_{0.9}PbI_3$**/spiro/Au	1.18	24.16	83.17	23.71	54
		1.17	24.08	83.06	23.40	
2022	ITO/SnO_2/**$FACsPbI_3$**/Spiro/Ag	1.11	23.04	78.75	20.84	55
		-	-	-	-	

Table S3. The average *J-V* parameters of 30 perovskite devices without and with ES.

	V_{OC} (V)	FF (%)	J_{SC} (mA·cm^{-2})	PCE (%)	R_S (Ω·cm^2)
Control	1.127	76.39	23.80	20.50	5.91
30 ES	1.175	78.98	23.81	22.08	3.27

Table S4. Parameters of the time-resolved photoluminescence (TRPL) spectroscopy, transient photocurrent (TPC) decay, and transient photovoltage (TPV) decay based on perovskite films without and with ES.

Characterizations		A_1	τ_1 (μs)	A_2	τ_2 (μs)	τ_{ave} (μs)
TRPL	Control	3.18	1.15×10^{-2}	0.71	0.205	0.167
	ES	0.32	0.151	0.57	0.573	0.518
TPC	Control	0.55	2.14	0.55	2.14	2.14
	ES	0.50	1.44	0.50	1.44	1.44

TPV	Control	0.73	10.6	0.29	31.1	21.6
	ES	0.91	13.7	0.17	77.0	46.1

Table S5. SCLC parameters of hole-only and electron-only devices based on control and ES perovskites.

Electron-only	V_{TFL} (V)	N_t ($10^{15}\cdot cm^{-3}$)	μ_e ($10^{-3}\cdot cm^2\cdot s^{-1}\cdot v^{-1}$)
Control	0.42	6.23	3.67
ES	0.20	2.97	3.14
Hole-only	V_{TFL} (V)	N_t ($10^{15}\cdot cm^{-3}$)	μ_h ($10^{-3}\cdot cm^2\cdot s^{-1}\cdot v^{-1}$)
Control	1.31	19.4	1.71
ES	1.03	15.3	2.47

Table S6. EIS parameters of the devices based on perovskite films without and with ES.

Voltage (V)	Control		ES	
	R_1 (Ω)	R_2 (Ω)	R_1 (Ω)	R_2 (Ω)
0	32.43	78162	93.11	34879
0.2	36.02	74491	64.12	25415
0.4	34.99	61879	57.87	20005
0.6	35.07	50429	44.06	15987
0.8	34.56	13167	45.64	9252

Table S7 Detailed photovoltaic parameters for PSCs in **Fig. 6c**.

	Time (h)	V_{OC} (V)	FF (%)	J_{SC} (mA·cm^{-2})	PCE (%)
Control	0	1.13	78.10	23.83	21.08
	48	1.14	75.24	23.58	20.20
	96	1.11	74.73	23.78	19.65
	144	1.11	71.81	23.78	18.95
	216	1.09	71.55	23.63	18.44
	264	1.08	69.94	23.45	17.77
	312	1.06	70.16	23.13	17.24
	360	1.05	68.59	23.02	16.57
	432	1.02	66.07	23.30	15.73
	504	1.00	65.03	22.70	14.82
	600	0.98	61.28	22.75	13.70
	672	0.98	55.90	22.67	12.46
	744	0.98	51.19	22.97	11.53
	840	0.96	50.98	22.88	11.14
	936	0.98	38.91	22.41	8.55
	1032	0.93	34.42	22.57	7.25
ES	0	1.17	80.45	23.83	22.39
	48	1.17	81.22	23.50	22.29
	96	1.17	78.32	23.86	21.94
	144	1.14	79.60	23.82	21.57
	216	1.15	78.98	23.47	21.33
	264	1.14	78.83	23.82	21.35
	312	1.13	80.25	23.37	21.20
	360	1.13	79.17	23.57	20.99
	432	1.12	79.31	23.52	20.82
	504	1.12	78.45	23.59	20.70
	600	1.11	77.77	23.89	20.64
	672	1.11	77.97	23.60	20.52
	744	1.11	78.15	23.42	20.28
	840	1.10	77.36	23.74	20.26
	936	1.11	76.78	23.71	20.13
	1032	1.09	77.41	23.76	19.95

Table S8 Photovoltaic parameters for control and ES-based PSCs stored in humidity air with RH 80±5%

Perovskite	Time (h)	V_{OC} (V)	FF (%)	J_{SC} (mA·cm^{-2})	PCE (%)	Normalized PCE (%)
Control	0	1.14	78.92	23.67	21.37	100
	24	1.10	56.21	22.98	14.28	66.8
	48	1.05	43.36	20.68	9.42	44.1
ES	0	1.18	79.08	23.99	22.32	100
	24	1.11	72.06	23.29	18.72	83.9
	48	1.10	57.84	22.74	14.59	65.4
	72	1.06	52.99	21.06	11.88	53.2

Table S9 Detailed photovoltaic parameters for PSCs in **Fig. 6d**.

	Time (h)	V_{OC} (V)	FF (%)	J_{SC} (mA·cm^{-2})	PCE (%)
Control	0	1.14	77.77	23.59	21.00
	24	1.14	78.06	23.68	21.07
	72	1.13	77.78	23.55	20.70
	120	1.12	77.72	23.31	20.35
	144	1.11	77.30	23.25	20.04
	216	1.10	75.41	23.28	19.26
	288	1.08	73.87	23.14	18.51
	360	1.05	71.76	23.10	17.49
	456	1.04	68.99	23.04	16.50
	528	1.02	66.27	23.07	15.63
	600	0.99	66.13	23.01	15.08
	696	0.93	65.95	22.80	14.08
	792	0.88	61.93	22.95	12.55
	888	0.85	59.34	22.77	11.46
	1056	0.82	50.26	21.68	8.94
ES	0	1.16	78.48	23.80	21.60
	24	1.16	79.38	23.80	21.95
	72	1.16	78.65	23.47	21.41
	120	1.15	77.48	23.59	21.08
	144	1.13	77.94	23.54	20.79
	216	1.13	77.07	23.50	20.50
	288	1.11	77.16	23.64	20.35
	360	1.11	77.23	23.48	20.20
	456	1.12	76.39	23.33	19.96
	528	1.10	76.25	23.19	19.47
	600	1.10	74.87	23.25	19.23
	696	1.10	74.20	23.22	18.92
	792	1.09	74.43	23.14	18.72
	888	1.07	74.70	23.15	18.59
	1056	1.08	73.81	23.11	18.39

References:

1. R. H. Yuan, B. Cai, Y. H. Lv, X. Gao, J. W. Gu, Z. H. Fan, X. H. Liu, C. Yang, M. Z. Liu and W. H. Zhang, *Energy Environ. Sci.*, 2021, **14**, 5074-5083.
2. G. Kresse and J. Furthmuller, *Phys. Rev. B*, 1996, **54**, 11169-11186.
3. P. E. Blochl, *Phys. Rev. B*, 1994, **50**, 17953-17979.
4. J. P. Perdew, K. Burke and M. Ernzerhof, *Phys. Rev. Lett.*, 1996, **77**, 3865-3868.
5. J. W. Wei, F. R. Huang, S. N. Wang, L. Y. Zhou, Y. L. Xin, P. Jin, Z. Cai, Z. D. Yin, Q. Pang and J. Z. Zhang, *Mater. Res. Bull.*, 2018, **106**, 35-39.
6. H. Zheng, X. Xu, S. Xu, G. Liu, S. Chen, X. Zhang, T. Chen and X. Pan, *Journal of Materials Chemistry C*, 2019, **7**, 4441-4448.
7. C. Liu, J. He, M. Wu, Y. Wu, P. Du, L. Fan, Q. Zhang, D. Wang and T. Zhang, *Solar Rrl*, 2020, **4**, 2000016.
8. Z. Li, M. Yang, J.-S. Park, S.-H. Wei, J. J. Berry and K. Zhu, *Chem. Mater.*, 2016, **28**, 284-292.
9. C. Yi, J. Luo, S. Meloni, A. Boziki, N. Ashari-Astani, C. Grätzel, S. M. Zakeeruddin, U. Röthlisberger and M. Grätzel, *Energy Environ. Sci.*, 2016, **9**, 656-662.
10. D. P. McMeekin, G. Sadoughi, W. Rehman, G. E. Eperon, M. Saliba, M. T. Horantner, A. Haghighirad, N. Sakai, L. Korte, B. Rech, M. B. Johnston, L. M. Herz and H. J. Snaith, *Science*, 2016, **351**, 151-155.
11. Y. Yu, C. Wang, C. R. Grice, N. Shrestha, J. Chen, D. Zhao, W. Liao, A. J. Cimaroli, P. J. Roland, R. J. Ellingson and Y. Yan, *ChemSusChem*, 2016, **9**, 3288-3297.
12. D. P. McMeekin, Z. Wang, W. Rehman, F. Pulvirenti, J. B. Patel, N. K. Noel, M. B. Johnston, S. R. Marder, L. M. Herz and H. J. Snaith, *Adv. Mater.*, 2017, **29**, 1607039.
13. W. Qiu, A. Ray, M. Jaysankar, T. Merckx, J. P. Bastos, D. Cheyns, R. Gehlhaar, J. Poortmans and P. Heremans, *Adv. Funct. Mater.*, 2017, **27**, 1700920.
14. Y. Zhou, F. Wang, Y. Cao, J.-P. Wang, H.-H. Fang, M. A. Loi, N. Zhao and C.-P. Wong, *Adv. Energy Mater.*, 2017, DOI: 10.1002/aenm.201701048, 1701048.
15. Y. Yu, C. Wang, C. R. Grice, N. Shrestha, D. Zhao, W. Liao, L. Guan, R. A. Awni, W. Meng, A. J. Cimaroli, K. Zhu, R. J. Ellingson and Y. Yan, *ACS Energy Lett.*, 2017, **2**, 1177-1182.
16. Y. Wu, P. Wang, S. Wang, Z. Wang, B. Cai, X. Zheng, Y. Chen, N. Yuan, J. Ding and W.-H. Zhang, *ChemSusChem*, 2018, **11**, 837-842.
17. J. Chen, J.-Y. Seo and N.-G. Park, *Adv. Energy Mater.*, 2018, DOI: 10.1002/aenm.201702714, 1702714.
18. J. Kim, M. I. Saidaminov, H. Tan, Y. Zhao, Y. Kim, J. Choi, J. W. Jo, J. Fan, R. Quintero-Bermudez, Z. Yang, L. N. Quan, M. Wei, O. Voznyy and E. H. Sargent, *Adv. Mater.*, 2018, **30**, 1706275.
19. H. W. Qiao, S. Yang, Y. Wang, X. Chen, T. Y. Wen, L. J. Tang, Q. Cheng, Y. Hou, H. Zhao and H. G. Yang, *Adv. Mater.*, 2018, **30**, 1804217.
20. S.-H. Turren-Cruz, A. Hagfeldt and M. Saliba, *Science*, 2018, **362**, 449-453.
21. Z. Wang, Q. Lin, B. Wenger, M. G. Christoforo, Y.-H. Lin, M. T. Klug, M. B. Johnston, L. M. Herz and H. J. Snaith, *Nat. Energy*, 2018, **3**, 855-861.
22. D. Yang, R. Yang, K. Wang, C. Wu, X. Zhu, J. Feng, X. Ren, G. Fang, S. Priya and S. Liu, *Nat. Commun.*, 2018, **9**, 3239.

23. H.-S. Yoo and N.-G. Park, *Solar Energy Materials and Solar Cells*, 2018, **179**, 57-65.
24. J. Chen, J. Xu, C. Zhao, B. Zhang, X. Liu, S. Dai and J. Yao, *ACS Appl. Mater. Interfaces*, 2019, **11**, 4597-4606.
25. G. Liu, H. Zheng, X. Xu, S. Xu, X. Zhang, X. Pan and S. Dai, *Adv. Funct. Mater.*, 2019, **29**, 1807565.
26. K. Schutt, P. K. Nayak, A. J. Ramadan, B. Wenger, Y. H. Lin and H. J. Snaith, *Adv. Funct. Mater.*, 2019, **29**, 1900466.
27. L. Xie, K. Lin, J. Lu, W. Feng, P. Song, C. Yan, K. Liu, L. Shen, C. Tian and Z. Wei, *J. Am. Chem. Soc.*, 2019, **141**, 20537-20546.
28. Z. Wu, Z. Liu, Z. Hu, Z. Hawash, L. Qiu, Y. Jiang, L. K. Ono and Y. Qi, *Adv. Mater.*, 2019, **31**, 1804284.
29. X. Hou, M. Xu, C. Tong, W. Ji, Z. Fu, Z. Wan, F. Hao, Y. Ming, S. Liu, Y. Hu, H. Han, Y. Rong and Y. Yao, *J. Power Sources*, 2019, **415**, 105-111.
30. S. Akin, E. Akman and S. Sonmezoglu, *Adv. Funct. Mater.*, 2020, **30**, 2002964.
31. J. Hou, F. Deng, Q. Wu, L. Yang, J. Wu, X. Li, Y.-Z. Zheng, N. Li, H. Ding and X. Tao, *J. Power Sources*, 2020, **449**, 227484.
32. Y. Chen, J. Yang, S. Wang, Y. Wu, N. Yuan and W.-H. Zhang, *iScience*, 2020, **23**, 100762.
33. S. Masi, C. Echeverría-Arrondo, K. M. M. Salim, T. T. Ngo, P. F. Mendez, E. López-Fraguas, D. F. Macias-Pinilla, J. Planelles, J. I. Climente and I. Mora-Seró, *ACS Energy Lett.*, 2020, **5**, 418-427.
34. J. Yang, Y. Chen, W. Tang, S. Wang, Q. Ma, Y. Wu, N. Yuan, J. Ding and W.-H. Zhang, *J. Energy Chem.*, 2020, **48**, 217-225.
35. X.-X. Gao, W. Luo, Y. Zhang, R. Hu, B. Zhang, A. Züttel, Y. Feng and M. K. Nazeeruddin, *Adv. Mater.*, 2020, **32**, 1905502.
36. Q. Yao, Q. Xue, Z. Li, K. Zhang, T. Zhang, N. Li, S. Yang, C. J. Brabec, H.-L. Yip and Y. Cao, *Adv. Mater.*, 2020, **32**, 2000571.
37. B. Liu, H. Bi, D. He, L. Bai, W. Wang, H. Yuan, Q. Song, P. Su, Z. Zang, T. Zhou and J. Chen, *ACS Energy Lett.*, 2021, **6**, 2526-2538.
38. M. Wang, S. Tan, Y. Zhao, P. Zhu, Y. Yin, Y. Feng, T. Huang, J. Xue, R. Wang, G. S. Han, H. S. Jung, J. Bian, J.-W. Lee and Y. Yang, *Adv. Funct. Mater.*, 2021, **31**, 2007520.
39. M. Fievez, P. J. S. Rana, T. M. Koh, M. Manceau, J. H. Lew, N. F. Jamaludin, B. Ghosh, A. Bruno, S. Cros, S. Berson, S. G. Mhaisalkar and W. L. Leong, *Sol. Energy Mater. Sol. Cells*, 2021, **230**, 111189.
40. S. B. Leng, L. Y. Wang, X. Wang, Z. F. Zhang, J. H. Liang, Y. T. Zheng, J. K. Jiang, Z. Zhang, X. Liu, Y. K. Qiu and C. C. Chen, *Solar Rrl*, 2021, **5**, 2100285.
41. D. M. Zheng, T. Zhu and T. Pauporte, *Solar Rrl*, 2021, **5**, 2100010.
42. P. Y. Su, L. Bai, H. Bi, B. B. Liu, S. Chen, D. Lee, H. Yang, C. Chen, Z. G. Zang and J. Z. Chen, *J. Power Sources*, 2021, **506**, 230213.
43. B. B. Liu, H. Bi, D. M. He, L. Bai, W. Q. Wang, H. K. Yuan, Q. L. Song, P. Y. Su, Z. G. Zang, T. W. Zhou and J. Z. Chen, *ACS Energy Lett.*, 2021, **6**, 2526-2538.
44. J. C. Yang, W. J. Tang, R. H. Yuan, Y. Chen, J. Wang, Y. H. Wu, W. J. Yin, N. Y. Yuan, J. N. Ding and W. H. Zhang, *Chem. Sci.*, 2021, **12**, 2050-2059.
45. T. Bu, J. Li, H. Li, C. Tian, J. Su, G. Tong, K. Ono Luis, C. Wang, Z. Lin, N. Chai, X.-L. Zhang, J. Chang, J. Lu, J. Zhong, W. Huang, Y. Qi, Y.-B. Cheng and F. Huang, *Science*, 2021,

372, 1327-1332.

46. Y. Li, Z. Chen, B. Yu, S. Tan, Y. Cui, H. Wu, Y. Luo, J. Shi, D. Li and Q. Meng, *Joule*, 2022, **6**, 676-689.
47. D. M. Zheng, T. Zhu, Y. F. Yan and T. Pauporte, *Adv. Energy Mater.*, 2022, **12**, 2103618.
48. L. Yang, J. S. Feng, Z. K. Liu, Y. W. Duan, S. Zhan, S. M. Yang, K. He, Y. Li, Y. W. Zhou, N. Y. Yuan, J. N. Ding and S. Liu, *Adv. Mater.*, 2022, **34**, 2201681.
49. H. Bi, Y. Guo, M. N. Guo, C. Ding, S. Hayase, T. Mou, Q. Shen, G. Y. Han and W. J. Hou, *Chem. Eng. J.*, 2022, **439**, 135671.
50. C. H. Wang, X. B. Wang, Z. H. He, B. Zhou, D. Qu, Y. Wang, H. W. Hu, Q. Hu and Y. G. Tu, *Chem. Eng. J.*, 2022, **444**, 136622.
51. T. Hou, M. Zhang, W. J. Yu, X. Wang, Z. Y. Gu, Q. Chen, L. Lan, X. R. Sun, Y. L. Huang, B. L. Zheng, X. Liu, M. A. Green and X. J. Hao, *J. Mater. Chem. A*, 2022, **10**, 2105-2112.
52. L. R. Li, Y. H. Lv, Q. L. Liu, Z. H. Fan, R. H. Yuan, W. J. Tang, X. H. Liu, P. Zhang and W. H. Zhang, *J. Mater. Chem. A*, 2022, **10**, 9161-9170.
53. S. Y. Wang, L. G. Tan, J. J. Zhou, M. H. Li, X. Zhao, H. Li, W. Tress, L. M. Ding, M. Graetzel and C. Y. Yi, *Joule*, 2022, **6**, 1344-1356.
54. Y. Q. Hu, Y. S. Shan, Z. L. Yu, H. J. Sui, T. Qiu, S. F. Zhang, W. Ruan, Q. F. Xu, M. M. Jiao, D. H. Wang, Y. Y. Wu, C. L. Yang and F. Xu, *J. Energy Chem.*, 2022, **64**, 561-567.
55. X. N. Sun, F. Deng, S. Q. Li, Y. Li, X. D. Lv, Y. Z. Zheng and X. Tao, *Solar Rrl*, DOI: 10.1002/solr.202200303, 11.